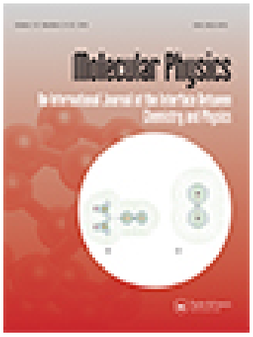

Molecular Physics

ISSN: 0026-8976 (Print) 1362-3028 (Online) Journal homepage: http://www.tandfonline.com/loi/tmph20

Relative equilibria of D_2H^+ and H_2D^+

I. N. KOZIN , R. M. ROBERTS & J. TENNYSON

To cite this article: I. N. KOZIN , R. M. ROBERTS & J. TENNYSON (2000) Relative equilibria of D_2H^+ and H_2D^+ , Molecular Physics, 98:5, 295-307, DOI: 10.1080/00268970009483293

To link to this article: http://dx.doi.org/10.1080/00268970009483293

Published online: 01 Sep 2009.

MOLECULAR PHYSICS, 2000, VOL. 98, NO. 5, 295–307

Relative equilibria of D_2H^+ and H_2D^+

I. N. KOZIN[1]*, R. M. ROBERTS[1] and J. TENNYSON[2]

[1]Mathematics Institute, University of Warwick, Coventry CV4 7AL, UK
[2]Department of Physics and Astronomy, University College London, London WC1E 6BT, UK

(*Received 29 July 1999; revised version accepted 14 September 1999*)

Relative equilibria of molecules are classical trajectories corresponding to steady rotations about stationary axes during which the shape of the molecule does not change. They can be used to explain and predict features of quantum spectra at high values of the total angular momentum J in much the same way that absolute equilibria are used at low J. This paper gives a classification of the symmetry types of relative equilibria of AB_2 molecules and computes the relative equilibria bifurcation diagrams and normal mode frequencies for D_2H^+ and H_2D^+. These are then fed into a harmonic quantization procedure to produce a number of predictions concerning the structures of energy level clusters and their rearrangements as J increases. In particular the formation of doublet pairs is predicted for H_2D^+ from $J \approx 26$.

1. Introduction

Relative equilibria play a central role in classical mechanics as organizing centres for more complex dynamics. They typically take the form of steady rotations about stationary axes during which the 'shape' of the system does not change. In applications to molecular spectroscopy they have previously been referred to as 'stationary points' [1, 2] or J-dependent reference points [3]. Unstable relative equilibria have also been studied in the guise of 'rotational' or 'centrifugal barriers' [4, 5] and 'transition states' [6]. Symmetry aspects related to relative equilibria have been discussed in the context of rotational energy surfaces [7, 8] and a detailed group theoretical analysis of relative equilibria of Rydberg states of atoms and molecules has been given in [9]. Dynamical symmetry breaking in H_2X molecules has also been formulated in terms of a modification of Longuet-Higgins' concept of feasible symmetry operations [10].

In a previous paper [11] we suggested that relative equilibria could be used systematically to explain and predict features of the quantum spectra of molecules at high values of the total angular momentum J in much the same way that ordinary (absolute) equilibrium points are used for $J = 0$ and, combined with perturbation theory, at low values of J. We also presented a complete bifurcation diagram of all the relative equilibria of H_3^+ and used this to predict a number of features in its energy spectrum.

In this paper we give a general analysis of AB_2 molecules and, in particular, of the two H_3^+ isotopomers D_2H^+ and H_2D^+. Our interest in J-dependent relative equilibria of these ions was stimulated by their possible importance in the context of predissociation spectra [12] in which very high rotational excitations are possible. Classical interpretations can also be of assistance in understanding the results of quantum variational calculations.

In section 2 of the paper we present the classical equations of motion of a molecule (in the Born–Oppenheimer approximation) and use these to show that relative equilibria are precisely the critical points of effective potential energy functions obtained by adding appropriate 'centrifugal potentials' to the molecular potential energy function. We then give the linearized equations of motion near a relative equilibrium. These are used later to compute normal mode frequencies and to determine stability properties. The modifications that are needed for linear configurations of molecules are also described. The final part of the section summarizes the harmonic quantization procedure introduced in [11]. For each relative equilibrium this yields estimates of the energies and symmetries of quantum states with wave functions localized near the relative equilibrium and its symmetry-equivalent counterparts.

In section 3 we give a complete classification of all possible symmetry types of relative equilibria of AB_2 molecules, distinguishing them by both their 'shape' and the orientation of their total angular momentum

* Author for correspondence. Permanent address: Institute of Applied Physics, Russian Academy of Sciences, Ulyanov St. 46, 603600 Nizhnii Novgorod, Russia.

vectors. The symmetry types of their normal modes and ground state are also listed. This is the data that is needed to determine the symmetries of localized quantum states in the harmonic quantization procedure.

These methods are applied to D_2H^+ in section 4 and to H_2D^+ in section 5. In both cases we have computed all the relative equilibria and the frequencies of their normal modes. The energies of the relative equilibria as functions of the total angular momentum J are presented in figures 1 and 4 up to $J = 70$. The normal mode frequencies for some of the linearly stable relative equilibria are presented in the other figures in sections 4 and 5. These results are then used to draw some conclusions about the existence of energy level clusters with particular multiplicities and symmetry types for specific ranges of total angular momentum values.

2. Classical equations of rovibrational motion

This section describes the classical equations of motion for molecules and derives from these the equations for its relative equilibria and the linearizations of the equations of motion at the relative equilibria. The methods used to analyse the stability of relative equilibria and to obtain harmonic quantization estimates from them are outlined.

2.1. *Nonlinear configurations*

With the standard choice of Euler angles [13], the kinetic energy of a nonlinear molecule with N nuclei takes the form

$$T = \tfrac{1}{2}\boldsymbol{\omega}^{\mathrm{T}}\mathbf{I}\boldsymbol{\omega} + \boldsymbol{\omega}^{\mathrm{T}}\mathbf{g}\dot{\mathbf{q}} + \tfrac{1}{2}\dot{\mathbf{q}}^{\mathrm{T}}\mathbf{a}\dot{\mathbf{q}}, \tag{1}$$

where $\mathbf{q}$ is the $3N-6$ dimensional vector of internal displacements, $\dot{\mathbf{q}}$ the corresponding vector of velocities, $\boldsymbol{\omega}$ the angular velocity, $\mathbf{I}$ the inertia tensor, $\mathbf{a}$ the reduced mass matrix and $\mathbf{g}$ the Coriolis interaction. This expression can be rearranged to give

$$T = \tfrac{1}{2}(\boldsymbol{\omega} + \mathbf{A}\dot{\mathbf{q}})^{\mathrm{T}}\mathbf{I}(\boldsymbol{\omega} + \mathbf{A}\dot{\mathbf{q}}) + \tfrac{1}{2}\dot{\mathbf{q}}^{\mathrm{T}}\mathbf{b}^{-1}\dot{\mathbf{q}}, \tag{2}$$

where $\mathbf{A} = \mathbf{I}^{-1}\mathbf{g}$ and $\mathbf{b}^{-1} = \mathbf{a} - \mathbf{g}^{\mathrm{T}}\mathbf{I}^{-1}\mathbf{g} = \mathbf{a} - \mathbf{A}^{\mathrm{T}}\mathbf{I}\mathbf{A}$. This splitting of the kinetic energy into two parts is gauge invariant, in other words it is independent of the choice of internal coordinates $\mathbf{q}$ [14]. The first term is the 'vertical' kinetic energy and can be taken to be a gauge independent definition of the rotational energy of the molecule while the second is a gauge independent definition of the 'horizontal' vibrational energy. In the language of [14] $\mathbf{A}$ is a gauge potential.

The canonical coordinates conjugate to $\boldsymbol{\omega}$ and $\mathbf{q}$ are

$$\mathbf{J} = \frac{\partial T}{\partial \boldsymbol{\omega}} = \mathbf{I}(\boldsymbol{\omega} + \mathbf{A}\dot{\mathbf{q}}), \tag{3}$$

$$\mathbf{p} = \frac{\partial T}{\partial \dot{\mathbf{q}}} = \mathbf{A}^{\mathrm{T}}\mathbf{J} + \mathbf{b}^{-1}\dot{\mathbf{q}}. \tag{4}$$

Here $\mathbf{J}$ is just the angular momentum in body coordinates. Substituting into equation (2) gives the Hamiltonian form of the kinetic energy

$$T = \tfrac{1}{2}\mathbf{J}^{\mathrm{T}}\mathbf{I}^{-1}\mathbf{J} + \tfrac{1}{2}(\mathbf{p} - \mathbf{A}^{\mathrm{T}}\mathbf{J})^{\mathrm{T}}\mathbf{b}(\mathbf{p} - \mathbf{A}^{\mathrm{T}}\mathbf{J}), \tag{5}$$

where again the first term is the rotational kinetic energy and the second the vibrational kinetic energy. The full Hamiltonian is obtained by simply adding the potential energy function $V(\mathbf{q})$ to this. Note that the Hamiltonian can also be expressed as the sum of the vibrational kinetic energy and the effective potential

$$V_{\mathbf{J}} = V + \tfrac{1}{2}\mathbf{J}^{\mathrm{T}}\mathbf{I}^{-1}\mathbf{J}. \tag{6}$$

In this context the rotational kinetic energy term is sometimes referred to as the centrifugal potential [14].

To obtain this form for the kinetic energy both the inertia tensor $\mathbf{I}$ and the matrix $\mathbf{a} - \mathbf{g}^{\mathrm{T}}\mathbf{I}^{-1}\mathbf{g} = \mathbf{a} - \mathbf{A}^{\mathrm{T}}\mathbf{I}\mathbf{A}$ are required to be invertible. The former condition holds precisely for nonlinear configurations of the molecule. Since $\mathbf{a}$ is always invertible the latter condition holds for configurations which are sufficiently close to one for which the internal coordinates satisfy the Eckart condition $\mathbf{g} = 0$, or equivalently $\mathbf{A} = 0$. Such internal coordinates can be chosen for any nonlinear configuration. Hamiltonians near linear configurations are discussed in the next subsection.

The equations of motion for the Hamiltonian $H = T + V$ with T given by equation (5) are

$$\begin{aligned}
\dot{\mathbf{J}} &= \mathbf{J} \times \frac{\partial H}{\partial \mathbf{J}} = \mathbf{J} \times (\mathbf{I}^{-1}\mathbf{J} - \mathbf{A}\mathbf{b}(\mathbf{p} - \mathbf{A}^{\mathrm{T}}\mathbf{J})), \\
\dot{\mathbf{q}} &= \frac{\partial H}{\partial \mathbf{p}} = \mathbf{b}(\mathbf{p} - \mathbf{A}^{\mathrm{T}}\mathbf{J}), \\
\dot{\mathbf{p}} &= -\frac{\partial H}{\partial \mathbf{q}} \\
&= -\frac{1}{2}\frac{\partial}{\partial \mathbf{q}}\Big((\mathbf{p} - \mathbf{A}^{\mathrm{T}}\mathbf{J})^{\mathrm{T}}\mathbf{b}(\mathbf{p} - \mathbf{A}^{\mathrm{T}}\mathbf{J})\Big) - \frac{\partial V_{\mathbf{J}}}{\partial \mathbf{q}}.
\end{aligned} \tag{7}$$

Relative equilibria are just equilibrium points of these equations and these are easily seen to be the solutions of the following system of equations

$$\begin{aligned}
\mathbf{I}^{-1}\mathbf{J} &= \lambda\mathbf{J}, \\
\frac{\partial V_{\mathbf{J}}}{\partial \mathbf{q}} &= 0, \\
\mathbf{p} &= {}^{\mathrm{T}}\,\mathbf{J},
\end{aligned} \tag{8}$$

for arbitrary λ. The first two equations involve only $\mathbf{J}$ and $\mathbf{q}$. Any solution of these determines a relative equilibrium by taking $\mathbf{p}$ to be given by the third equation. Thus we can conclude that a relative equilibrium always rotates about a principal axis of its configuration, and the configuration is a critical point of the effective potential for the corresponding value of $\mathbf{J}$. Note that for a triatomic molecule the principal axes, and hence the rotation axes and angular momentum vectors, must either lie in the molecular plane or be perpendicular to it.

This suggests a very simple recipe of finding molecular relative equilibria. Take the potential function, find the inertia tensor from geometrical properties of the molecule, form the effective potentials with $\mathbf{J}$ parallel to the principal axes of the inertia tensor and search for their stationary points.

The absolute value J of the total angular momentum $\mathbf{J}$ is an integral of motion and so the number of independent equations in (7) is actually $(6N-10)$ where N is number of nuclei in the molecule. Therefore the number of degrees of freedom in the reduced ro-vibrational problem is $(3N-5)$. The value J of the total angular momentum can be regarded as a parameter.

To obtain the linearized equations at a relative equilibrium we assume that internal coordinates have been chosen so that the Eckart condition $\mathbf{A}=0$ is satisfied at the relative equilibrium. The values of the variables $(\mathbf{J},\mathbf{q},\mathbf{p})$ at the relative equilibrium are denoted $(\mathbf{J}_e,\mathbf{q}_e,0)$ and infinitesimal perturbations from these values are written $\mathbf{J}=\mathbf{J}_e+\boldsymbol{\xi}\times\mathbf{J}_e$, $\mathbf{q}=\mathbf{q}_e+\mathbf{s}$ and $\mathbf{p}=\boldsymbol{\sigma}$, where $\boldsymbol{\xi}$ is a vector in the plane perpendicular to $\mathbf{J}_e$. Let $\hat{\mathbf{J}}_e$ denote the 2×3 matrix which satisfies $\hat{\mathbf{J}}_e\boldsymbol{\xi}=\mathbf{J}_e\times\boldsymbol{\xi}$. Let $\mathbf{A}_\mathbf{J}=\mathbf{J}^\mathrm{T}\mathbf{A}$. Then with respect to the variables $(\boldsymbol{\xi},\mathbf{s},\boldsymbol{\sigma})$ the second derivative, or Hessian, of the Hamiltonian is given by:

$$\begin{pmatrix} \hat{\mathbf{J}}_e^\mathrm{T}\mathbf{I}^{-1}\hat{\mathbf{J}}_e & -\hat{\mathbf{J}}_e^\mathrm{T}\mathbf{C} & 0 \\ -\mathbf{C}^\mathrm{T}\hat{\mathbf{J}}_e & \mathbf{U} & -\mathbf{B}\mathbf{a}^{-1} \\ 0 & -\mathbf{a}^{-1}\mathbf{B}^\mathrm{T} & \mathbf{a}^{-1} \end{pmatrix}, \tag{9}$$

where $\mathbf{I}^{-1}$ and

$$\mathbf{C}=\frac{\partial^2 V_\mathbf{J}}{\partial\mathbf{J}\partial\mathbf{q}},\qquad \mathbf{U}=\frac{\partial^2 V_\mathbf{J}}{\partial\mathbf{q}^2},\qquad \mathbf{B}=\frac{\partial\mathbf{A}_\mathbf{J}}{\partial\mathbf{q}}$$

are all evaluated at the relative equilibrium. The linearized equations of motion are:

$$\begin{pmatrix}\dot{\boldsymbol{\xi}}\\ \dot{\mathbf{s}}\\ \dot{\boldsymbol{\sigma}}\end{pmatrix}=\begin{pmatrix}(\mathbf{I}^{-1}-\lambda_e I)\hat{\mathbf{J}}_e & -\overline{\mathbf{C}} & 0\\ 0 & -\mathbf{a}^{-1}\mathbf{B}^\mathrm{T} & \mathbf{a}^{-1}\\ \mathbf{C}^\mathrm{T}\hat{\mathbf{J}}_e & -\mathbf{U} & \mathbf{B}\mathbf{a}^{-1}\end{pmatrix}\begin{pmatrix}\boldsymbol{\xi}\\ \mathbf{s}\\ \boldsymbol{\sigma}\end{pmatrix}, \tag{10}$$

where $\overline{\mathbf{C}}$ is the projection of $\mathbf{C}$ to the plane perpendicular to $\mathbf{J}_e$, I is the identity matrix and λ_e is the principal moment of inertia of the configuration about the axis parallel to $\mathbf{J}_e$. Equivalently these equations can be written as:

$$\dot{\boldsymbol{\xi}}-(\mathbf{I}^{-1}-\lambda_e I)\hat{\mathbf{J}}_e\boldsymbol{\xi}=-\overline{\mathbf{C}}\mathbf{s}, \tag{11}$$

$$\mathbf{a}\ddot{\mathbf{s}}+(\mathbf{B}^\mathrm{T}-\mathbf{B})\dot{\mathbf{s}}+(\mathbf{U}-\mathbf{B}\mathbf{a}^{-1}\mathbf{B}^\mathrm{T})\mathbf{s}=\mathbf{C}^\mathrm{T}\hat{\mathbf{J}}_e\boldsymbol{\xi}. \tag{12}$$

Note that $\mathbf{B}^\mathrm{T}-\mathbf{B}$ is skew-symmetric while $\mathbf{U}-\mathbf{B}\mathbf{a}^{-1}\mathbf{B}^\mathrm{T}$ is symmetric. A calculation shows that $\mathbf{U}-\mathbf{B}\mathbf{a}^{-1}\mathbf{B}^\mathrm{T}$ is the Hessian of the *modified* potential $V+\mathbf{J}^\mathrm{T}\boldsymbol{\mu}\mathbf{J}$ at the relative equilibrium, where $\boldsymbol{\mu}$ is the inverse of $\mathbf{I}-\mathbf{g}\mathbf{a}^{-1}\mathbf{g}^\mathrm{T}$.

A relative equilibrium is linearly stable if the four normal mode frequencies determined by equation (10) are all real. Note that in general the precessional motion is coupled to the internal vibrations though the Coriolis interaction and it does not always make sense to distinguish the precessional mode from the vibrational modes. In some cases symmetries force $\overline{\mathbf{C}}=0$, in which case the precessional mode is decoupled from the others.

To each normal mode of equation (10) we can assign an index 1, -1 or 0 as follows. A stable normal mode for which the energy increases as its amplitude grows is labelled by 1, one for which the energy decreases by -1, and an unstable normal mode by 0. A relative equilibrium is a local minimum of the energy if its normal modes all have the index 1. In this case it is Liapunov stable: all trajectories with initial conditions close to the relative equilibrium remain close to it for all time. A relative equilibrium which is not a local minimum may still be linearly stable, though typically it will not be Liapunov stable as nearby classical trajectories may slowly drift away from the relative equilibrium as a result of Arnold diffusion [15].

2.2. *Linear configurations*

In the case of perturbations from linear molecules the transformation to internal coordinates described above becomes singular because the inertia tensor $\mathbf{I}$ has a zero eigenvalue at the linear reference configuration. Moreover an extra coordinate is required to describe the internal displacements of the molecule, making $\mathbf{q}$ into a $3N-5$ dimensional vector. To compensate for this only two independent Euler angles are used [16]. We choose the z axis for the molecular coordinate system to be the principal axis direction parallel to the linear reference configuration. The two Euler angles are the angles which describe this direction in space. This restricts $\boldsymbol{\omega}$ to be two dimensional, $\boldsymbol{\omega}_\mathrm{lin}=(\omega_x,\omega_y)$, and we can replace the inertia tensor $\mathbf{I}$ by

$$\mathbf{I}_\mathrm{lin}=\begin{pmatrix}I_{xx} & I_{xy}\\ I_{xy} & I_{yy}\end{pmatrix}$$

and the $3 \times (3N-6)$ Coriolis interaction matrix $\mathbf{g}$ by a $2 \times (3N-5)$ matrix $\mathbf{g}_{\text{lin}}$. We may now proceed as in the nonlinear case. The matrix $\mathbf{I}_{\text{lin}}$ is invertible and the kinetic energy (2) becomes [16]

$$T = \tfrac{1}{2}(\boldsymbol{\omega}_{\text{lin}} + \mathbf{A}_{\text{lin}}\dot{\mathbf{q}})^{\mathrm{T}}\mathbf{I}_{\text{lin}}(\boldsymbol{\omega}_{\text{lin}} + \mathbf{A}_{\text{lin}}\dot{\mathbf{q}}) + \tfrac{1}{2}\dot{\mathbf{q}}^{\mathrm{T}}\mathbf{b}^{-1}\dot{\mathbf{q}}, \quad (13)$$

where $\mathbf{A}_{\text{lin}} = \mathbf{I}_{\text{lin}}^{-1}\mathbf{g}_{\text{lin}}$ and $\mathbf{b}^{-1} = \mathbf{a} - \mathbf{A}_{\text{lin}}^{\mathrm{T}}\mathbf{I}_{\text{lin}}\mathbf{A}_{\text{lin}}$. As in the nonlinear case the internal coordinates can be assumed to satisfy the Eckart condition $\mathbf{A}_{\text{lin}} = 0$ at the linear configuration and so $\mathbf{b}$ is well defined.

Momentum coordinates $\mathbf{J}_{\text{lin}}$ and $\mathbf{p}$ are defined by equations (3) and (4) with $\boldsymbol{\omega}$, $\mathbf{I}$ and $\mathbf{A}$ replaced by $\boldsymbol{\omega}_{\text{lin}}$, $\mathbf{I}_{\text{lin}}$ and $\mathbf{A}_{\text{lin}}$. The vector $\mathbf{J}_{\text{lin}} = (J_x, J_y)$ continues to give the x and y components of the angular momentum in molecular coordinates. The z component is equal to the projection of the 'vibrational angular momentum' onto the z axis, $J_z = (\mathbf{g}\mathbf{a}^{-1}\mathbf{p})_z$. This is known as the Sayvetz condition. The Hamiltonian form of the kinetic energy becomes

$$T = \tfrac{1}{2}\mathbf{J}_{\text{lin}}^{T}\mathbf{I}_{\text{lin}}^{-1}\mathbf{J}_{\text{lin}} + \tfrac{1}{2}(\mathbf{p} - \mathbf{A}_{\text{lin}}^{\mathrm{T}}\mathbf{J}_{\text{lin}})^{\mathrm{T}}\mathbf{b}(\mathbf{p} - \mathbf{A}_{\text{lin}}^{\mathrm{T}}\mathbf{J}_{\text{lin}}). \quad (14)$$

The first term may still be regarded as the vertical kinetic energy and the second as the horizontal kinetic energy. The full Hamiltonian H_{lin} is obtained by adding the potential energy V to this and may therefore be written as the sum of the horizontal kinetic energy and an effective potential $V_{\mathbf{J}_{\text{lin}}}$ defined as in (6) with $\mathbf{J}_{\text{lin}}$ and $\mathbf{I}_{\text{lin}}$ replacing $\mathbf{J}$ and $\mathbf{I}$.

The equations of motion for the internal variables $(\mathbf{q}, \mathbf{p})$ are completely analogous to those given in (7). Those for $\mathbf{J}_{\text{lin}} = (J_x, J_y)$ become:

$$\begin{pmatrix} \dot{J}_x \\ \dot{J}_y \end{pmatrix} = J_z \begin{pmatrix} 0 & -1 \\ 1 & 0 \end{pmatrix} \begin{pmatrix} \dfrac{\partial H_{\text{lin}}}{\partial J_x} \\ \dfrac{\partial H_{\text{lin}}}{\partial J_y} \end{pmatrix}$$

$$= (\mathbf{g}\mathbf{a}^{-1}\mathbf{p})_z \begin{pmatrix} 0 & -1 \\ 1 & 0 \end{pmatrix} \times (\mathbf{I}_{\text{lin}}^{-1}\mathbf{J}_{\text{lin}} - \mathbf{A}_{\text{lin}}\mathbf{b}(\mathbf{p} - \mathbf{A}_{\text{lin}}^{\mathrm{T}}\mathbf{J}_{\text{lin}})). \quad (15)$$

It is easily seen that equilibrium points of the full set of equations of motion must satisfy either $J_x = J_y = 0$ or $J_z = 0$. In the first case they must also be critical points of the original potential V, and so can only be equilibrium points of the full molecular Hamiltonian. However the second case yields non-trivial relative equilibria, the shapes of which are given by critical points of the effective potential $V_{\mathbf{J}_{\text{lin}}}$. For these relative equilibria the axial symmetry of the effective potential implies that the direction of the total angular momentum $\mathbf{J}$ can be anywhere in the xy plane.

When the equations of motion are linearized at a linear relative equilibrium it is found that $\dot{J}_x = \dot{J}_y$ and the $3N-5$ normal mode frequencies are all given by the linearized equations for $\mathbf{q}$ and $\mathbf{p}$:

$$\begin{pmatrix} \dot{\mathbf{s}} \\ \dot{\boldsymbol{\sigma}} \end{pmatrix} = \begin{pmatrix} -\mathbf{a}^{-1}\mathbf{B}^{\mathrm{T}} & \mathbf{a}^{-1} \\ -\mathbf{U} & \mathbf{B}\mathbf{a}^{-1} \end{pmatrix} \begin{pmatrix} \mathbf{s} \\ \boldsymbol{\sigma} \end{pmatrix} \quad (16)$$

or, equivalently

$$\ddot{\mathbf{s}} + (\mathbf{B}^{\mathrm{T}} - \mathbf{B})\dot{\mathbf{s}} + (\mathbf{U} - \mathbf{B}\mathbf{a}^{-1}\mathbf{B}^{\mathrm{T}})\mathbf{s} = 0, \quad (17)$$

where

$$\mathbf{U} = \frac{\partial^2 V_{\mathbf{J}_{\text{lin}}}}{\partial \mathbf{q}^2} \quad \text{and} \quad \mathbf{B} = \frac{\partial(\mathbf{J}_{\text{lin}}^{\mathrm{T}}\mathbf{A}_{\text{lin}})}{\partial \mathbf{q}},$$

evaluated at the relative equilibrium.

2.3. *Harmonic quantization*

The energies of quantum states which are localized near linearly stable relative equilibria are given approximately by the harmonic quantization formula [11]:

$$E_{n_1 \ldots n_d} = E_{\text{re}}(J) + \sum_{l=1}^{d} k_l \omega_l(J)\left(n_l + \frac{1}{2}\right), \quad (18)$$

where $E_{\text{re}}(J)$ is the energy of the relative equilibrium, n_l is the number of quanta in the lth normal mode, $\omega_l(J)$ is its frequency, k_l its stability index and $d = 3N-5$ is the number of degrees of freedom. A better correspondence with the quantum energy levels is obtained by replacing J by $[J(J+1)]^{1/2}$. This estimate ignores anharmonic corrections and also the splitting due to tunnelling between symmetry equivalent relative equlibria. It will clearly only be useful for wave functions which are localized near to the relative equilibrium.

Approximate wave functions localized near a relative equilibrium can be labelled according to how they transform under the molecular symmetry group of the relative equilibrium [11]. A wave function with n_l quanta in the lth normal mode will have symmetry type

$$\Gamma^{\text{loc}}_{n_1 \ldots n_d} = \Gamma_0 \otimes \Gamma_1^{n_1} \otimes \ldots \otimes \Gamma_d^{n_d}, \quad (19)$$

where Γ_0 is the symmetry of the ground state of the relative equilibrium, i.e. the wave function with zero normal mode quanta, Γ_l is the representation of the symmetry group on the lth normal mode, $\otimes$ denotes the (tensor) product of representations and $\Gamma_l^{n_l}$ is the product of Γ_l with itself n_l times. From the correspondence principle in the classical limit the ground state of the relative equilibrium must be the product of ground state wave functions in each normal mode and the symmetric top wave function $|J\ K = J\ M\rangle$, where the quantization axis is chosen along the axis of steady rotation of the relative equilibrium [17]. Since ground state wave

functions of normal modes are locally symmetric, the local symmetry type is determined by the actions of equivalent rotations [18] of the molecular symmetry group of the relative equilibrium on $|J\ K = J\ M\rangle$ and in general will vary with J.

Symmetry equivalent relative equilibria have symmetry equivalent wave functions which interact with each other via tunnelling. The resulting wave functions of the quantum states of the molecule given by harmonic approximation are linear combinations of the localized wave functions and can be labelled by how they transform under the full molecular symmetry group of the molecule. The representation of this group on the space of all quantum states obtained in this way from a single localized wave function of type $\Gamma^{\text{loc}}_{n_1 \ldots n_d}$ is the corresponding induced representation. These are most conveniently calculated using Frobenius reciprocity [11] or, equivalently, the reverse correlation technique [18]. In general these representations are reducible and the energies of the irreducible components are split by tunnelling, giving rise to energy level clusters with characteristic symmetry properties. The structures of some of these clusters for relative equilibria of AB_2 molecules are described in the next section.

3. Symmetries of relative equilibria of AB_2 molecules

In this section we give the symmetry groups of all possible types of relative equilibria of AB_2 molecules and describe the appropriate symmetry labelling of approximate wave functions localized near each type. Our notation for molecular symmetry groups will follow that of [18] except where explicitly stated otherwise.

3.1. *The group* $C_{2v}(\mathrm{M})$

In molecular coordinates the Hamiltonian of an AB_2 molecule is invariant under the permutation-inversion group $C_{2v}(\mathrm{M}) = \{E, (12), E^*, (12)^*\}$ where (12) denotes the permutation of the two identical nuclei, E^* is inversion and $(12)^*$ is their composition. The representations of this group can be found elsewhere [18]. Occasionally, for example when considering linear configurations, it is more convenient to interpret this group as the isomorphic $C_{2h}(\mathrm{M})$ but we will use the $C_{2v}(\mathrm{M})$ group only. We denote the subgroups of order two of $C_{2v}(\mathrm{M})$ by

$$C_2(\mathrm{M}) = \{E, (12)\},$$

$$C_s(\mathrm{M}) = \{E, E^*\},$$

$$C_i(\mathrm{M}) = \{E, (12)^*\}.$$

To simplify notation we always denote the totally symmetric representations of these groups by A and the other representations by B. In table 1 we show the representations of $C_{2v}(\mathrm{M})$ that are obtained by induction from A and B for each of the order two subgroups. The final column shows the representation obtained by induction from the trivial representation of the trivial group $\{E\}$.

Table 1. The representations of $C_{2v}(\mathrm{M})$ obtained by induction from its subgroups.

	$C_2(\mathrm{M})$	$C_s(\mathrm{M})$	$C_i(\mathrm{M})$	$\{E\}$
A	$A_1 + A_2$	$A_1 + B_2$	$A_1 + B_1$	$A_1 + A_2 + B_1 + B_2$
B	$B_1 + B_2$	$A_2 + B_1$	$A_2 + B_2$	–

3.2. *Equilibria*

There are four possible types of equilibrium configurations of an AB_2 molecule, symmetric linear (SL), asymmetric linear (AL), isosceles triangle (IT) and asymmetric triangle (AT). The SL and IT equilibria are both invariant under the full symmetry group $C_{2v}(\mathrm{M})$ while the AL and AT equilibria are only invariant under $C_s(\mathrm{M})$. It follows that AL and AT equilibria form symmetry equivalent pairs. The normal mode symmetries for each of these equilibrium types are

$$\mathrm{SL}: A_1 + A_2 + 2B_2, \qquad \mathrm{AL}: 3A + B,$$

$$\mathrm{IT}: 2A_1 + B_2, \qquad \mathrm{AT}: 3A.$$

Note that the doubly degenerate bending modes of SL and AL equilibria 'split' into $A_2 + B_2$ and $A + B$ representations of their molecular symmetry groups. The degeneracy is therefore due to spatial symmetries and not permutation-inversion symmetries. The effects of these extra symmetries can be captured using 'extended' molecular symmetry groups $D_{\infty h}(\mathrm{EM})$ and $C_{\infty v}(\mathrm{EM})$ [18], however these symmetries disappear when we consider relative equilibria and so we do not need to use extended symmetry groups in this paper.

3.3. *Relative equilibria*

The possible configurations of relative equilibria are the same as those for equilibria, namely SL, AL, IT and AT. However two relative equilibria with the same configuration may rotate about different molecular axes, and thus have differently oriented total angular momentum vectors. For linear configurations the angular momentum vectors must be perpendicular to the linear axis and so there is only one type of symmetric linear and one type of asymmetric linear relative equilibrium. We continue to denote these by SL and AL, respectively.

We saw in section 2.1 that a relative equilibrium with a nonlinear configuration must rotate about one of its principal axes. Accordingly the IT relative equilibria

Table 2. Symmetry types of relative equilibria of AB_2 molecules.

Label	Local symmetry group	No.	Vibrational normal modes	Prec. norm. mode	Ground state	
					J even	J odd
SL	$C_{2v}(M)$	1	$A_1 + A_2 + 2B_2$	–	A_1	B_1
AL	$C_s(M)$	2	$3A + B$	–	A	B
IT^y	$C_s(M)$	2	$3A$	B	A	B
IT^x	$C_2(M)$	2	$2A + B$	B	A	B
IT^z	$C_i(M)$	2	$2A + B$	B	A	B
AT^y	$C_s(M)$	4	$3A$	B	A	B
AT^{xz}	$\{E\}$	4	–	–	–	–

come in three different symmetry types, IT^γ, where $\gamma = x, y$ or z denotes the rotation axis. For AT configurations there are no symmetries to distinguish between different directions in the molecular plane and so an AT relative equilibrium can either have the rotation axis perpendicular to the molecular plane, AT^y, or lying in the molecular plane, AT^{xz}.

The local permutation-inversion symmetry groups of each of the different types of relative equilibria are given in the second column of table 2. The table also lists the representations of these groups on the vibrational normal modes, the precessional normal modes of non-linear configurations and on the ground states of the relative equilibria (see section 2.3). Note that in each case the ground state is totally symmetric when J is even, but has non-trivial symmetries when J is odd.

The third column in the table shows the number of distinct symmetry-related relative equilibria that must accompany a relative equilibrium of each type. In each case except AT^y the number is equal to 4, the order of $C_{2v}(M)$, divided by the order of the local symmetry group. To understand the exceptional case note that the molecular Hamiltonian is also invariant under the time-reversal operation which multiplies all momenta by -1. This operation maps each SL and AL relative equilibrium to itself, but in all other cases maps a relative equilibrium to a different relative equilibrium. We include relative equilibria which are mapped to each other by time-reversal symmetry in the definition of 'symmetry-related' relative equilibria. In the IT^γ and AT^{xz} cases time reversal maps a relative equilibrium to another relative equilibrium that can also be obtained from a permutation-inversion symmetry, so no extra relative equilibria are obtained. However in the AT^y case time reversal maps a relative equilibrium to a different relative equilibrium than those that are obtained from the permutation-inversion symmetries.

Note that the three different types of relative equilibria with $C_s(M)$ local permutation-inversion symmetry groups, namely AL, IT^y and AT^y, can be distinguished by their time-reversal symmetry properties. The AL relative equilibria are mapped to themselves, the IT^y relative equilibria to distinct permutation-inversion symmetry-related relative equilibria and AT^y relative equilibria to otherwise unrelated relative equilibria. The quantum consequences of these different time-reversal symmetry properties will be explored elsewhere. In this paper our labelling of quantum levels will make use of the $C_{2v}(M)$ permutation-inversion symmetry group only.

3.4. *Cluster symmetry types*

Tables 1 and 2 together give all the information that is needed to determine the possible symmetry types of clusters of energy levels predicted by harmonic quantization at relative equilibria. The symmetry types of wave functions localized near a single relative equilibrium are given by equation (19) with the appropriate entries from table 2 substituted for the Γ_j. The induced cluster representations are then given by table 1. The dimension of the cluster representation is always equal to the number of symmetry-related relative equilibria. Thus the energy levels associated to the SL relative equilibria will be non-degenerate, while the others will be either doublets (AL and IT relative equilibria) or quadruplets (AT relative equilibria).

As an example we consider clusters associated to IT^y relative equilibria. The local symmetry type of an approximate wave function with all n quanta in a single symmetric normal mode is A if J is even and B if J is odd. The corresponding induced cluster types are $A_1 + B_2$ and $A_2 + B_1$, respectively. If all n quanta are in the (asymmetric) precessional mode then the local symmetry type is A if $J + n$ is even and B if $J + n$ is odd and the cluster types are again $A_1 + B_2$ and $A_2 + B_1$, respectively.

If time-reversal symmetry is ignored the local symmetry types for AT^y relative equilibria are the same as those for IT^y relative equilibria and so the induced

cluster symmetry types are also the same. The effect of the time-reversal symmetry is to 'double-up' the eigenspaces. Thus for symmetric (resp. asymmetric) normal modes the cluster representations are $2A_1 + 2B_2$ and $2A_2 + 2B_1$ for J (resp. $J + n$) even and odd. The AT^{xz} quadruplets always have symmetry type $A_1 + A_2 + B_1 + B_2$.

4. Relative equilibria of D_2H^+

In the next two sections we describe the relative equilibria of the two isotopomers D_2H^+ and H_2D^+ of H_3^+ and make some predictions about associated spectral patterns. The numerical calculations assume an isolated ground electronic state, use the potential function of Dinelli *et al.* [19] and neglect non-adiabatic corrections. Thus the only differences between the Hamiltonians used here for D_2H^+ and H_2D^+ and in [11] for H_3^+ are the masses of the nuclei. For both D_2H^+ and H_2D^+ the relative equilibria are found by solving for the critical points of appropriate effective potentials V_J and $V_{J_{lin}}$ using the MATHEMATICA computer package [20]. Plots of the energies of the relative equilibria as functions of J are given as figures 1 and 4. The normal mode frequencies for each of the relative equilibria were calculated using equations (10) and (16), again with MATHEMATICA. Plots of the normal mode frequencies for the linearly stable relative equilibria are shown in a series of figures in this section for D_2H^+ and in the next section for H_2D^+. The rest of this section describes the bifurcations of relative equilibria that occur for D_2H^+ and their associated spectral consequences, while the next section does the same for H_2D^+.

4.1. *Bifurcations of relative equilibria*

The relative equilibrium bifurcation diagram for D_2H^+ up to $J = 70$ is shown in figure 1. At low energies for $J < 50$ the only relative equilibria are isosceles triangles rotating about each of their three principal axes. The IT^y relative equilibria have minimum energy and so have stability index (1111) and are both linearly and nonlinearly stable. The IT^z relative equilibria are also linearly stable, but with stability index (111−1) and are likely to be unstable over long time periods as a result of Arnold diffusion. The IT^x relative equilibria have stability index (1110) and so are both linearly and nonlinearly unstable. As J increases centrifugal forces elongate the IT^z relative equilibria, reducing the angle between the two HD bonds, until at $J \approx 50$ they finally disappear in a bifurcation with branches of 'rotational barrier' relative equilibria of the same symmetry type which come in from infinity. However before this happens the IT^z relative equilibria lose stability in a Hamiltonian Hopf bifurcation [11, 21] at $J \approx 37$. In other words the frequencies of two normal modes

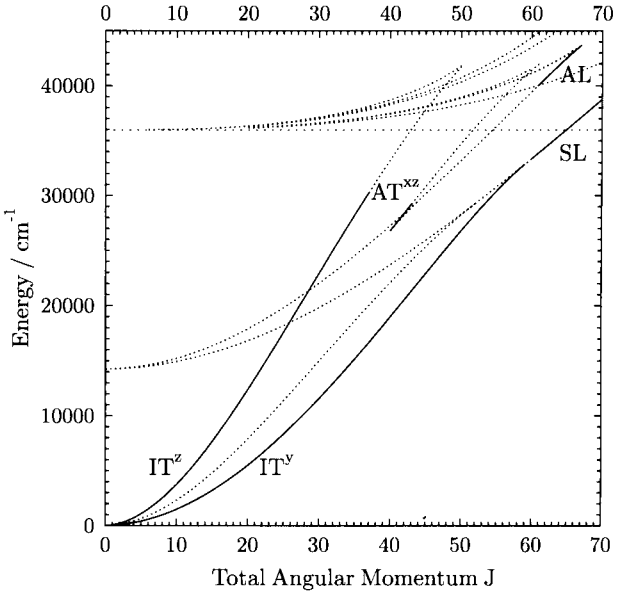

Figure 1. The energies of linearly stable (—) and unstable (···) relative equilibria of the D_2H^+ ion as functions of the total angular momentum J. The linearly stable configurations are labelled by IT for isosceles triangle, AT for asymmetric triangle, SL for symmetric linear and AL for asymmetric linear. The superscripts indicate the direction of the angular momentum vector. The horizontal dotted line denotes the first dissociation energy of the ion to two products.

become equal at the bifurcation point and thereafter form a complex conjugate pair. This changes the stability index to (1100).

For both the IT^x and IT^y relative equilibria the centrifugal forces act to increase the angle between the two HD bonds until, at $J \approx 50$ and $J \approx 59$ respectively, they become linear. These two bifurcations stabilize the SL relative equilibria which start out at low values of J with stability index (1100), along with branches of AL relative equilibria. The SL go on to lose stability again in a bifurcation to AL relative equilibria at $J \approx 90$ (not shown in figure 1) before eventually colliding with matching rotational barriers.

At $J \approx 39$ there is a fold bifurcation which gives birth to a pair of branches of AT^{xz} relative equilibria with stability indices (111−1) and (1110). The linearly stable branch loses stability soon afterwards in a Hamiltonian Hopf bifurcation and is unlikely to have any observable influence on spectra. The unstable branch collides with the AL relative equilibria, raising their stability, and these are then stabilized in a bifurcation with AT^y at $J \approx 61$. However both the AL and AT^y relative equilibria quickly disappear in collisions with matching rotational barriers and again no observable effects on the spectrum are likely. The energies of the AT^y relative

equilibria are so close to those of the AL relative equilibria that they are indistiguishable in figure 1.

4.2. *Normal modes and spectral clusters*

The normal mode frequencies of IT^z relative equilibria are shown in figure 2. The two key features are a Hamiltonian Hopf bifurcation involving the anti-symmetric precessional and stretching modes at $J \approx 37$ and a close avoided crossing between the two symmetric vibrational modes at $J \approx 25$. It follows from the discussion of section 26 that as the IT^z relative equilibria have symmetry group $C_i(M)$ the associated quantum energy level doublets will be of types $A_1 + B_1$ and $A_2 + B_2$. Excited symmetric modes will always be of type $A_1 + B_1$ if J is even and type $A_2 + B_2$ if J is odd. The avoided crossing will result in many resonances between these around $J \approx 25$. Excited anti-symmetric modes will give doublets of type $A_1 + B_1$ for even numbers of quanta and $A_2 + B_2$ for odd numbers when J is even and the opposite for J odd. Since the precessional mode has stability index -1 the corresponding energy levels will decrease in energy as the numbers of quanta increase. The effects of the Hamiltonian Hopf bifurcation on these patterns remain to be investigated.

The normal mode frequencies of the IT^y relative equilibria are given in figure 3 up to $J \approx 60$, where the relative equilibria 'become linear'. All the vibrational modes are symmetric with respect to the local symmetry group $C_s(M)$ while the precessional mode is anti-symmetric. There is therefore no interaction between the precessional and vibrational modes. The most notable feature is that the lowest frequency mode changes from precessional to a bending vibrational mode at $J \approx 41$. The frequency of the latter goes to zero at the bifurcation point from the SL relative equilibria. The normal mode frequencies of SL relative equilibria are given in the same figure for the range $J \approx 60 - 90$ in which they are stable. The A_1 mode is the symmetric stretching mode, the A_2 mode consists of bending oscillations in the plane containing the total angular momentum vector and the B_2 modes are linear combinations of asymmetric stretching and bending in the plane perpendicular to the total angular momentum vector. The lowest frequency B_2 mode changes from a bending oscillation near $J = 60$ to a stretching oscillation near $J = 90$.

The $C_s(M)$ symmetry group of IT^y relative equilibria implies that the associated energy level doublets are of types $A_1 + B_2$ and $A_2 + B_1$. For low values of J the low energy spectrum will consist of excited precessional states with the alternating sequence of $A_1 + B_2$ and $A_2 + B_1$ doublets for J even, reversed for J odd, typical of rigid rotors. This should change for $J > 40$ when the lowest frequency becomes vibrational and consequently the associated doublets will all have the same type as the

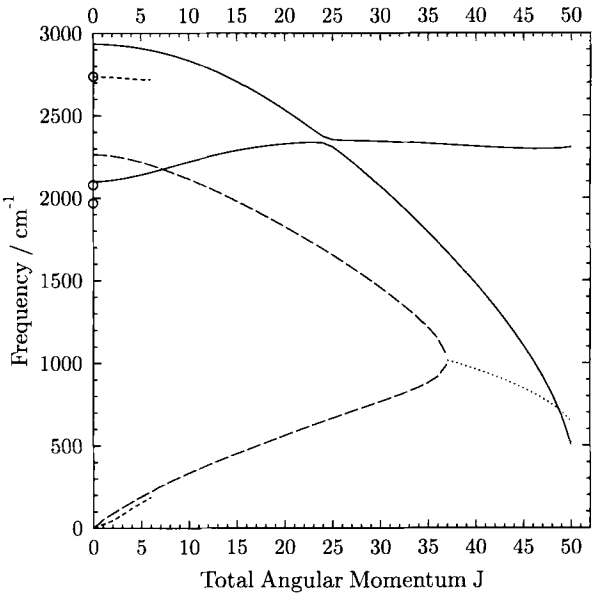

Figure 2. Classical normal mode frequencies for the IT^z RE of the D_2H^+ ion. Solid lines correspond to modes which are symmetric with respect to $C_i(M)$, large dashed lines to modes which are anti-symmetric and the small dashed line shows the real part of the complex frequency after the Hamiltonian Hopf bifurcation at $J \approx 37$. Short dash lines represent estimates of classical frequencies from quantum calculations [23]. Circles indicate experimental vibrational frequencies [22, 23].

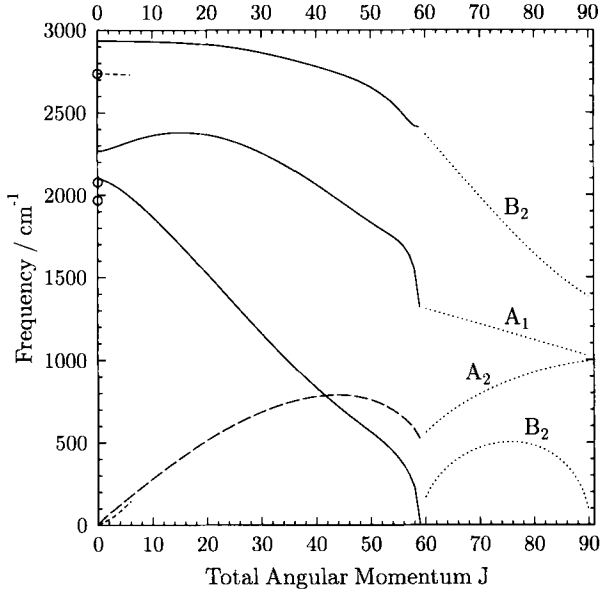

Figure 3. Classical normal mode frequencies for the IT^y and SL relative equilibria of the D_2H^+ ion. Solid lines correspond to symmetric IT^y modes, the large dashed line to the anti-symmetric IT^y precessional mode and individually labelled dotted lines to the SL normal modes. Short dash lines represent estimates of classical frequencies from quantum calculations [23]. Circles indicate experimental vibrational frequencies [22, 23].

ground state. However, the precessional frequency is still very close and the next excited doublet should be precessional.

The frequencies of the IT^y relative equilibria transform continuously into the frequencies of the SL relative equilibria. However, the changes to the quantum spectrum will be more pronounced. The symmetry groups of the SL relative equilibria are the full permutation-inversion group of the molecule and there are no distinct symmetry equivalent relative equilibria. It follows that the energy levels should be singlets and we expect to see a splitting of energy level doublets as J passes through 60. The symmetry of the ground state for SL relative equilibria is A_1 for J even and B_1 for J odd. The lowest frequency normal mode is B_2 and so for $J > 60$ the two lowest energy states will have symmetries A_1 and B_2 when J is even and B_1 and A_2 when J is odd.

5. H_2D^+

5.1. *Bifurcations of relative equilibria*

The energies of the relative equilibria of H_2D^+ are shown as functions of J up to $J = 70$ in figure 4. The bifurcation diagram is rather more complicated than that for D_2H^+ and we concentrate on describing some of the key differences. First note that at low J it is the IT^x relative equilibria that are linearly stable, instead of the IT^z relative equilibria. These lose stability in a bifurcation to AT^{xz} relative equilibria at $J \approx 20$ before becoming linear at $J \approx 36$. The AT^{xz} relative equilibria

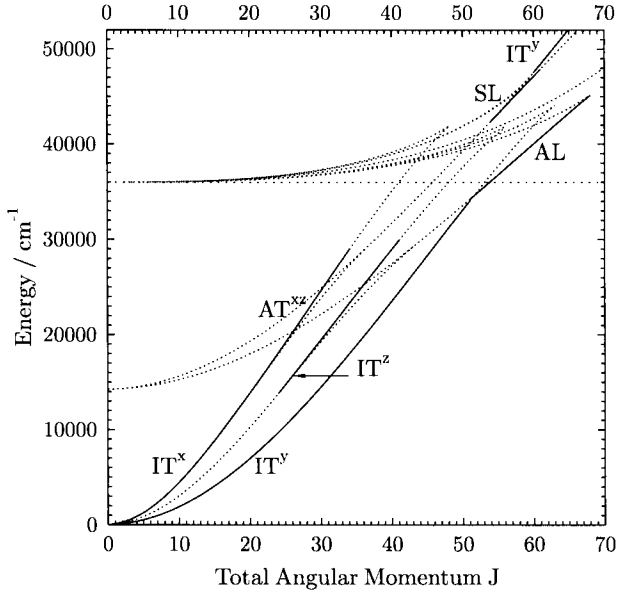

Figure 4. The energies of linearly stable (—) and unstable (···) relative equilibria of the H_2D^+ ion as functions of the total angular momentum J. The labelling is the same as in figure 1.

themselves lose stability in a Hamiltonian Hopf bifurcation at $J \approx 33$ and then disappear in a collision with rotational barriers. The unstable IT^z become stable at $J \approx 24$ as a result of a bifurcation to another branch of (unstable) AT^{xz} relative equilibria. The IT^z relative equilibria go on to lose stability again in a Hamiltonian Hopf bifurcation at $J \approx 41$ and then collide with rotational barriers at $J \approx 55$.

In contrast to D_2H^+ the AL relative equilibria have lower energies than the SL relative equilibria. The AL relative equilibria are stabilized as J increases by a bifurcation to AT^{xz} relative equilibria at $J \approx 41$, followed by an exchange of stabilities with the minimal energy IT^y relative equilibria at $J \approx 51$. This exchange also involves a branch of AT^y relative equilibria that is not visible in the figure. As a result the IT^y relative equilibria lose stability and the AL relative equilibria become the minimum energy configurations. To begin with the AL relative equilibria give the absolute minimum of the energy, but from $J \approx 53$ they are only a local minimum above the dissociation energy. Both the AL and the IT^y relative equilibria go on to collide with matching rotational barriers, at $J \approx 68$ and $J \approx 63$, respectively.

The higher energy SL relative equilibria are also stabilized by a pair of bifurcations, first to IT^x relative equilibria at $J \approx 34$ and then to another branch of IT^y relative equilibria at $J \approx 54$. The SL relative equilibria lose stability again in a bifurcation to AL relative equilibria at $J \approx 61$ while just before this the IT^y relative equilibria become stable as a result of a bifurcation to AT^y relative equilibria. The IT^y relative equilibria lose stability in a Hamiltonian Hopf bifurcation at $J \approx 74$ (not shown) before colliding with its rotational barrier. These are the (linearly) stable relative equilibria with both the highest energy and the highest angular momentum.

5.2. *Normal modes and spectral clusters*

The analysis of energy level clusters associated to linearly stable relative equilibria of H_2D^+ proceeds exactly as for D_2H^+. Here we concentrate on features associated with the IT^x to AT^{xz} and the IT^y to AL bifurcations of relative equilibria.

The normal mode frequencies for the IT^x relative equilibria in their stable range $J \approx 0 - 20$ and for the AT^{xz} relative equilibria in the range $J \approx 20 - 49$ are given in figure 5. The IT^x local symmetry group is $C_2(M)$ and so the associated energy level doublets will be of types $A_1 + A_2$ and $B_1 + B_2$. The four-fold multiplicity of AT^{xz} relative equilibria implies that they will have energy level quadruplets of symmetry type $A_1 + A_2 + B_1 + B_2$. Thus as J passes through 20 there should be a merging of pairs of doublets of complementary symmetry type to form quadruplets.

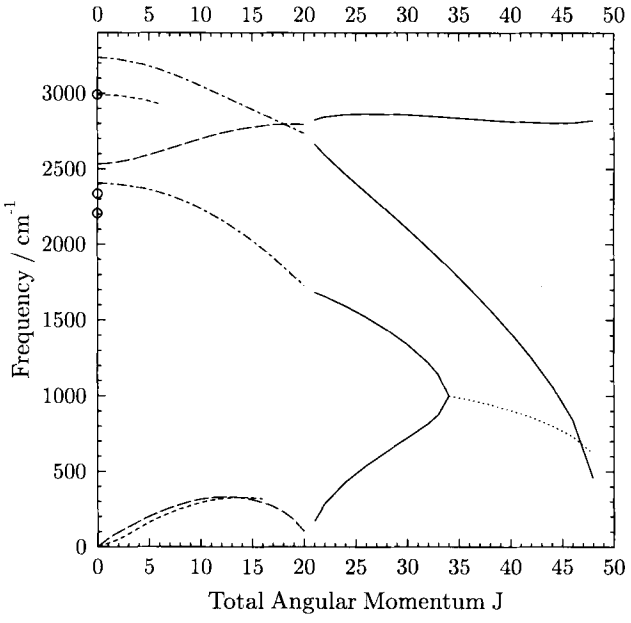

Figure 5. Classical normal mode frequencies of the IT^x and AT^{xz} relative equilibria of the H_2D^+ ion. Dash-dot lines correspond to the symmetric modes of IT^x, large dashed lines to the anti-symmetric modes, solid lines to the normal mode frequencies of AT^{xz} and the dotted line shows the real part of the complex frequency of AT^{xz} after the Hamiltonian Hopf bifurcation at $J \approx 34$. Short dash lines represent estimates of classical frequencies from quantum calculations [23, 24]. Circles indicate experimental vibrational frequencies [23, 25].

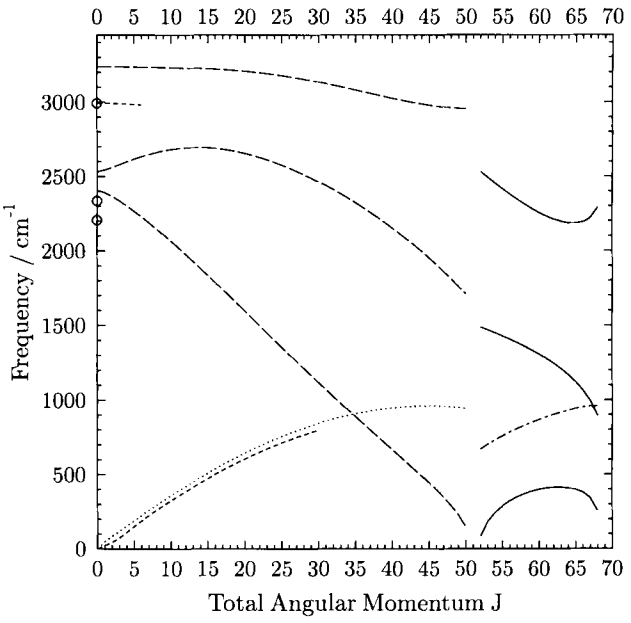

Figure 6. The classical normal mode frequencies for IT^y and AL relative equilibria of the H_2D^+ ion for the values of J for which they are linearly stable. The dashed lines correspond to symmetric IT^y, the dotted line to the anti-symmetric IT^y precessional mode, the solid lines to the symmetric AL modes and the dash-dot line to the anti-symmetric AL mode. Short dash lines represent estimates of classical frequencies from quantum calculations [23, 24]. Circles indicate experimental vibrational frequencies [23, 25].

The normal mode frequencies of the IT^y relative equilibria in their stable range $J \approx 0 - 50$ are given in figure 6, followed by the normal mode frequencies of the AL relative equilibria in their stable range $J \approx 50 - 68$. As for D_2H^+, symmetries prevent the IT^y precessional mode from interacting with the vibrational modes in harmonic approximation. There is also a similar switch in the lowest frequency mode from precessional to vibrational, and this will be accompanied by a similar rearrangement of $A_1 + B_2$ and $A_2 + B_1$ doublets. In this case it is likely to be more distinct as there is a greater separation between the precessional frequency and the lowest vibrational frequency. However, the main difference between the two cases comes when the ions 'go linear'. In this case the transition is to AL relative equilibria which appear in pairs and so will continue to be accompanied by doublets. Moreover the local symmetry groups of IT^y and AL relative equilibria are the same, C_s(M), and so their clusters will have the same symmetry types. It is therefore likely that the transition from IT^y to AL structure will not be observable in the quantum spectrum.

6. Summary and discussion

We have described a general method for computing the relative equilibria of a molecule and their normal modes. The symmetry classification of all the possible relative equilibria and their associated 'harmonic' quantum states has been given for an arbitrary AB_2 molecule. The possible applications of these results to specific molecules are illustrated using the examples of D_2H^+ and H_2D^+. All the relative equilibria types listed in table 2 exist for each of these examples, and almost all of them are linearly stable for some range of angular momentum values. The only exceptions are IT^x for D_2H^+ and AT^y for both D_2H^+ and H_2D^+. In general we expect a linearly stable relative equilibrium to act as an organizing centre for families of quantum states with wave functions which are localized near it and its symmetry equivalent counterparts. Tunelling will create clusters of energy levels of symmetry types which are characteristic of the symmetry type of the relative equilibrium and bifurcations of the relative equilibrium may lead to rearrangements of these clusters.

Despite having the same potential function, the relative equilibrium bifurcation diagrams of H_3^+, D_2H^+ and

H_2D^+ are quite different. The differences are dictated to a large extent by the symmetries of the ions and the role of the centrifugal forces. Yet there are some common features, for example the stabilization of linear configurations as J increases. This is well known [4, 26] and is perhaps a general phenomenon of AB_2 molecules. Here we have shown that both symmetric and asymmetric linear configurations can be stabilized and that either can occur as the global minimum of the total energy. In the case of D_2H^+ the transition to a symmetric linear (SL) global minimum occurs at $J \approx 59$. For H_2D^+ it is the AL configurations which become global minima of the energy, in this case at $J \approx 51$. Their energy increases above the dissociation level at $J \approx 53$. Linearly stable SL relative equilibria exist above dissociation for $J \approx 54 - 61$. Moreover in this case, as for H_3^+ [11], there are also linearly stable relative equilibria with triangular configurations above dissociation.

In [11] we predicted that for H_3^+ the transition to linear geometry will be accompanied by a rearrangement of energy level doublets associated to equilateral triangle relative equilibria to form triplets associated with symmetric linear configurations. The results of this paper show that for D_2H^+ the transition will be accompanied by a splitting of the energy level doublets of types $A_1 + B_2$ and $A_2 + B_1$ associated with the minimal energy IT^y relative equilibria to give singlets associated with the SL geometry. The difference is due to the lower permutational symmetry group of D_2H^+. Since the AL and IT^y relative equilibria have the same symmetry group the corresponding transition for H_2D^+ may have little effect on the spectrum.

Another common feature of all the ions is that the lowest excited level changes from rotational to vibrational as J increases. It happens most quickly in H_3^+ where the precessional frequency exceeds the smallest vibrational normal mode at $J = 30$ [11]. This value is 35 for H_2D^+. The highest value is 42 for D_2H^+ and the effect here is probably the least likely to be observed because the precessional and vibrational frequencies are too close.

Perhaps the most likely event to be detected in the quantum spectrum is the bifurcation from IT^x to AT^{xz} relative equilibria in H_2D^+. This should be accompanied by a merging of pairs of energy level doublets of types $A_1 + A_2$ and $B_1 + B_2$ to form quadruplets. This bifurcation is somewhat unusual for AB_2 molecules. In most cases rotation about the x axis is unstable and the IT^x relative equilibrium can simply 'become linear' without any change in stability as the BAB bond angle increases. However, because of the initially small bond angle, rotation about the x axis is stable for H_2D^+ at low values of J, but becomes unstable as J and the angle increase. Similar bifurcations, though with decreasing bond angles, do occur from IT^z relative equilibria for a number of AB_2 molecules [27]. In this case theoretical predictions [1, 2, 28, 29] have been confirmed by full quantum mechanical calculations [30, 31] and experimentally for H_2Se [32], H_2Te [33] and H_2S [34]. These bifurcations are also accompanied by merging of pairs of doublets. The value of J for which the IT^x bifurcation occurs in H_2D^+ is higher than that for the IT^z bifurcations in H_2Se, H_2Te, comparable with that in H_2S and lower than expected in H_2O [35]. For H_2D^+ the IT^z relative equilibria also undergo a bifurcation but the mechanism underlying this is not so easily explained and must be a more subtle interaction between the potential and centrifugal effects.

The harmonic approximation used above is rather poor in terms of high resolution spectroscopy when estimating pure vibrational frequencies since the anharmonic effects are very strong in D_2H^+ and H_2D^+: the normal modes at $J = 0$ overestimate the experimental frequencies by 7–9% (see circles in figures 2, 3, 5 and 6). However, it is still instructive to compare the present calculations with available experimental and calculated data. For instance, it is clear from figure 2 that there must be a strong $\Delta K_a = 1$ resonance at low J in D_2H^+ between the levels of the ν_2 mode (the lowest symmetric one) and the levels of the asymmetric ν_3 mode having one additional precessional quantum (recall that the precessional mode in IT^z descends in energy). This is not the case in H_2D^+ for which ν_2 and ν_3 always diverge (see figures 5 and 6). Indeed, Foster *et al.* [22] noted in the experimental analysis of D_2H^+ that they had to add a K_a-dependent interaction term and drop a J-dependent term compared to their H_2D^+ model [25] when fitting similar data. Similarly one can predict a number of other resonances of which the most notable is the avoided crossing again in IT^z of D_2H^+ between ν_1 and ν_3 at $J \approx 25$. Interestingly this feature resembles the crossing in H_2D^+ at slightly lower values of J (see figure 5).

It is often straightforward to correlate the classical normal mode frequencies to a quantum spectrum. For example, the energy differences $E(K_a = J) - E(K_a = J - 1)$ correlate with the precessional frequency of the IT^x relative equilibrium of H_2D^+ and $E(K_c = J - 1) - E(K_c = J)$ with the precessional frequency of IT^y. These J dependences of characteristic frequencies present another way of comparing our classical calculations with experiment. Unfortunately the assigned experimental data are very limited ($J \leqslant 6$) [22, 25]. The observed predissociation spectra of D_2H^+ and H_2D^+ should have very high J, especially when kinetic energy release is high [12] but these spectra still remain unassigned in detail. The only extensive source of assigned levels known to us is [24] where the assignment of the ground vibrational state of H_2D^+, obtained

from quantum variational calculations, has been given up to $J = 30$. Another source is the calculation of energy levels in the ground and ν_1 states of H_2D^+ and D_2H^+ based on the effective Hamiltonian fitted to experimental data [23].

The quantum data obtained in this way are presented in the respective figures of the normal modes. One can see that apart from the strong anharmonic shifts the J dependences are reproduced rather well. For precessional modes the classical frequency again gives an upper boundary for quantum levels. The relative error comes down to less than 6% for IT^y relative equilibrium of H_2D^+ at $J = 30$. For IT^x the classical estimates are also close to the quantum but become lower starting from $J = 14$, 'foreseeing' the bifurcation. This is however not unusual since the quantum difference is somewhat more 'inertial'. Quantum mechanically the merging of two doublets is due to the tunnelling effect between equivalent relative equilibria. But the tunnelling takes place only if the height of a separation barrier is higher than at least the ground state of the relative equilibrium. We can estimate the ground state energy as half of the precessional frequency (see equation (18)) and compare it with the barrier height. The barrier exceeds the ground state for $J > 26$. When this happens in H_2Se or H_2S the ratio between the cluster width and the space to the next level is 1:4 [35]. Therefore we can hope that $J \approx 26$ gives us an estimate of the point above which cluster features may be observed in the spectrum of H_2D^+. However, there is a complication due to the Hamiltonian Hopf bifurcation at $J \approx 33$. Energetically this happens below the barrier which suggests that cluster features may be perturbed but persist. To verify this a detailed analysis is required.

The analogous comparisons of classical and quantum data for D_2H^+ illustrate mostly how little we know about this ion. With recent advances in variational methods it is becoming feasible to carry out more extensive calculations which should clarify the quantum structure of high ro-vibrational levels in H_2D^+ and D_2H^+ and particularly show if the formation of four-fold clusters of levels takes place in H_2D^+ and what happens to them in the Hamiltonian Hopf bifurcation.

We are grateful to Boris Zhilinskii for a number of very useful discussions. This work was supported by a UK EPSRC research grant. INK also thanks partial support from the Russian Fund for Fundamental Research through grant No 97-02-16593.

References

[1] ZHILINSKII, B. I., and PAVLICHENKOV, I. M., 1988, *Opt. Spectrosc.* (USSR), **64,** 413.
[2] KOZIN, I. N., and PAVLICHENKOV, I. M., 1996, *J. chem. Phys.*, **104,** 4105.
[3] LOHR, L. L., 1996, *Int. J. quantum Chem.*, **57,** 707.
[4] BERBLINGER, M., POLLAK, E., and SCHLIER, CH., 1988, *J. chem. Phys.*, **88,** 5643.
[5] CHAMBERS, A. V., and CHILD, M. S., 1988, *Molec. Phys.*, **65,** 1337.
[6] MILLER, M. A., and WALES, D. J., 1996, *Molec. Phys.*, **89,** 534.
[7] HARTER, W. G., and PATTERSON, C. W., 1984, *J. chem. Phys.*, **43,** 4241.
[8] HARTER, W. G., 1993, *Principles of Symmetry, Dynamics and Spectroscopy* (New York: Wiley).
[9] MICHEL, L., and ZHILINSKII, B., 1997, Technical Report No. IHES/P/97/54 (France: Institute des Hautes Etudes Scientifiques Bures-sur-Yvette).
[10] JENSEN, P., and BUNKER, P. R., 1994, *J. molec. Spectrosc.*, **164,** 315.
[11] KOZIN, I. N., ROBERTS, R. M., and TENNYSON, J., 1999, *J. chem. Phys.*, **111,** 140.
[12] CARRINGTON, A., and KENNEDY, R., 1984, *J. chem. Phys.*, **81,** 91; CARRINGTON, A., MCNAB, I. R., and WEST, Y. D., 1992, *J. chem. Phys.*, **98,** 1073.
[13] WILSON JR, E. B., DECIUS, J. C., and CROSS, P. C., 1955, *Molecular Vibrations* (New York: McGraw-Hill Book Company).
[14] LITTLEJOHN, R. G., and REINSCH, M., 1997, *Rev. mod. Phys.*, **69,** 213.
[15] ARNOLD, V. I., KOZLOV, V. V., and NEISHTADT, A. I., 1997, *Mathematical Aspects of Classical Mechanics* (Berlin, Heidelberg: Springer Verlag), Ch. 5.
[16] WATSON, J. K. G., 1970, *Molec. Phys.*, **19,** 465.
[17] WIGNER, E. P., 1968, *Group Theory and Its Application to the Quantum Mechanics of Atomic Spectra* (London: Academic Press).
[18] BUNKER, P. R., and JENSEN, P., 1998, *Molecular Symmetry and Spectroscopy* (Ottawa: NRC Research Press).
[19] DINELLI, B. M., POLYANSKY, O. L., and TENNYSON, J., 1995, *J. chem. Phys.*, **103,** 10433.
[20] WOLFRAM RESEARCH, INC., 1996, *Mathematica*, Version 3.0 (Champaign, IL: Wolfram Research, Inc.).
[21] VAN DER MEER, J. C., 1985, *Lecture Notes in Mathematics*, Vol. 1160 (Berlin: Springer-Verlag).
[22] FOSTER, S. C., MCKELLAR, A. R. W., and WATSON, J. K. G., 1986, *J. chem. Phys.*, **85,** 664.
[23] KOZIN, I. N., POLYANSKY, O. L., and ZOBOV, N. F., 1988, *J. molec. Spectrosc.*, **128,** 126.
[24] POLYANSKY, O. L., MILLER, S., and TENNYSON, J., 1993, *J. molec. Spectrosc.*, **157,** 237.
[25] FOSTER, S. C., MCKELLAR, A. R. W., PETERKIN, I. R., WATSON, J. K. G., PAN, F. S., CROFTON, M. W., ALTMAN, R. S., and OKA, T., 1986, *J. chem. Phys.*, **84,** 91.
[26] POLLAK, E., 1987, *J. chem. Phys.*, **86,** 1645.
[27] JENSEN, P., OSMANN, G., and KOZIN, I. N., 1997, *Advanced Series in Physical Chemistry: Vibration-Rotational Spectroscopy and Molecular Dynamics*, edited by D. Papousek (Singapore: World Scientific Publishing Co.).
[28] MAKAREWICZ, J., 1998, *J. chem. Phys.*, **108,** 469 and references therein.
[29] LEHMANN, K. K., 1991, *J. chem. Phys.*, **95,** 2361.
[30] KOZIN, I. N., and JENSEN, P., 1993, *J. molec. Spectrosc.*, **161,** 186; 1993, *ibid.*, **163,** 483.

[31] JENSEN, P., LI, Y., HIRSCH, G., BUENKER, R. J., LEE, T. J., and KOZIN, I. N., 1994, *Chem. Phys.*, **190,** 179.
[32] KOZIN, I. N., KLEE, S., JENSEN, P., POLYANSKY, O. L., and PAVLICHENKOV, I. M., 1993, *J. molec. Spectrosc.*, **158,** 409.
[33] KOZIN, I. N., JENSEN, P., POLANZ, O., KLEE, S., POTEAU, L., and DEMAISON, J., 1996, *J. molec. Spectrosc.*, **180,** 402.
[34] BYKOV, A. D., NAUMENKO, O. V., SMIRNOV, M. A., SINITSA, L. N., BROWN, L. R., CRISP, J., and CRISP, D., 1994, *Can. J. Phys.*, **72,** 989; VAITINEN, O., BIENNIER, L., CAMPARGUE, A., FLAUD, J.-M., and HALONEN, L., 1997, *J. molec. Spectrosc.*, **184,** 288.
[35] KOZIN, I. N., and PAVLICHENKOV, I. M., 1997, *JETP*, **85,** 673.